

Estimating Precision in Functional Images

Ranjan Maitra *

Abstract

Functional imaging of biologic parameters like *in vivo* tissue metabolism is made possible by Positron Emission Tomography (PET). Many techniques have been suggested for extracting such images from dynamic time-course sequences of reconstructed PET scans. Quantitating the precision of these estimates is important for drawing inferences on the biologic parameters. Analytic variance formulae are not immediate owing to the nonlinear methods used in extraction. The usual resampling approach is infeasible because each image reconstruction in PET is a computationally demanding solution to a high-dimensional linear inverse problem. We suggest an alternative simulation approach which approximates the distribution of reconstructed PET scans and performs a parametric bootstrap in the imaging domain. Results on a simplified model chosen to match the characteristics of PET reconstruction are very encouraging. Mixture analysis is used to estimate functional images; however, the suggested approach is general enough to extend to other techniques or imaging methods.

Keywords: PET, bootstrap, radio-tracer, source distribution, Radon transform, generalized linear model, Filtered Backprojection, convolution, Fast Fourier transform, Toeplitz matrix, multivariate Gaussian distribution, TAC, sub-TAC, mixture analysis, variable-span smoother.

1 Introduction

Positron Emission Tomography [17] is a radiologic tool used to image biologic function of tissue. The imaging protocol consists of injecting a patient with a radio-tracer and recording the emissions at discrete time-points. From emissions recorded at each time-point, the tissue isotope concentration or *source distribution* is estimated, giving us a time-course sequence of re-

constructed PET scans. These scans form the input for algorithms that output pixel-wise estimates of biologic parameters like metabolic rate, phosphorylation ratio, etc. Such images are called functional images and the potential to quantitate these is the most powerful feature of PET.

Assessing precision of the estimated functional images is important for making inferences like calculating significance levels of tests of hypothesis on biologic activities in different regions. The problem of developing practical variability measures for reconstructed PET scans at fixed time-points has been studied extensively ([3],[7],[8]). Blomqvist *et al.* [2] noted the desirability of extending these results to functional images. Unfortunately, the nonlinear formulations used in constructing the parameter estimates make analytic variance formulae intractable. Extending the simulation approach of Haynor and Woods [7] is impractical because of the excessive computational effort required to reconstruct dynamic PET sequences.

In this paper, we suggest a simulation approach via the parametric bootstrap [5] executed in the imaging domain. We prove that with increased count rate, each reconstructed PET scan has an approximate multivariate Gaussian distribution. The mean is estimated by the reconstructed image. Computationally feasible and accurate dispersion estimates are suggested. This model is used to simulate dynamic PET sequences, from each of which biologic parameters are extracted. This yields a bootstrap sample of the functional images, which can be used to assess variability. The advantage of this approach over the usual one is that it eliminates the computationally expensive step of reconstructing time-course sequences after simulating from the observation process.

The main contributions of this paper are presented in two sections. Section 2 specifies the approximate distribution of a PET scan. Results on a simulated PET experiment are reported. Section 3 investigates the problem of assessing variability in functional images estimated from dynamic PET scans by mixture analysis. Since it is not possible to validate our methods in a two-dimensional PET setup, the suggestions are evaluated on experiments performed in a model one-dimensional deconvolution problem with similar characteristics to PET. Finally, Section 4 summarizes

*Ranjan Maitra is Research Scientist in the Statistics and Data Analysis Research Group, Bellcore, Morristown, NJ 07960, USA; e-mail: maitra@bellcore.com. This work was supported in part by the National Institutes of Health under CA-57903, and primarily done while he was a Ph. D. student in the Department of Statistics at the University of Washington, Seattle.

the contributions of this paper and poses questions for future research.

2 Distribution of a PET scan

2.1 Theory and Methods

2.1.1 Reconstruction

In PET, observations can be regarded as a realization of an inhomogeneous Poisson Process with rates that are linear combinations of the source distribution. ([16],[18]). Denote the number of pixels in the imaging domain by I and the number of detector bins by J . Let also $\lambda = \{\lambda_i; i = 1, 2, \dots, I\}$ denote the source distribution and $\mu = \{\mu_j; j = 1, 2, \dots, J\}$ be the rate parameters in the observation domain, with $y = \{y_j; j = 1, 2, \dots, J\}$ the recorded counts. In this setting, $\mu = K\lambda$, where K is a linear integral operator – approximately a Radon transform. Then, the reconstruction problem may be formulated as that of finding the coefficients λ of the generalized linear model,

$$\mathbb{E}(y_j) = K_j \lambda, \quad j = 1, 2, \dots, J \quad (1)$$

where K_j represents the j 'th row of K . The least-squares solution after smoothing with a Gaussian kernel S_h of pre-specified bandwidth h is,

$$\hat{\lambda}^h = S_h(K'K)^{-1}K'y \equiv E_h y \quad (2)$$

where $E_h = S_h(K'K)^{-1}K'$ is a $I \times J$ matrix. Since the detectors record the observations in terms of angle, θ , and distance, d , writing the j 'th detector bin in terms of its corresponding distance-angle representation, the reconstruction at the i 'th pixel is,

$$\hat{\lambda}_i^h = e_i^h y = \sum_{\theta=1}^{n_\theta} \sum_{d=1}^{n_d} e_{i,d,\theta}^h y_{d,\theta} \quad (3)$$

where e_i^h denotes the i 'th row of E_h , $i = 1, 2, \dots, I$, n_θ the number of discretized angles in the detector space and n_d the number of distances. Denoting the position of the i 'th pixel by the coordinates $\{u_i, v_i\}$, $i = 1, 2, \dots, I$, the e^h 's in PET have a functional form $e_{i,d,\theta}^h = e_h(u_i \cos \theta + v_i \sin \theta - d)$. Hence, (3) can be rewritten as

$$\hat{\lambda}_i^h = \sum_{\theta=1}^{n_\theta} \sum_{d=1}^{n_d} e_h(u_i \cos \theta + v_i \sin \theta - d) y_{d,\theta} \quad (4)$$

From (4), we note that source distributions may be estimated by first convolving the data $\{y\}$ from each projection angle with the kernel $\{e_h(\cdot)\}$ and then backprojecting (summing the contributions) onto the

imaging domain. This method is called *Filtered Back-projection*. Two points need mention here : (1) The convolution is speedily done by Fast Fourier Transforms and backprojection is the computationally greedy step. (2) There are several more sophisticated reconstruction algorithms; however, the relative superior computational efficiency of this method has resulted in it being the most commonly used.

2.1.2 Approximate Distribution of $\hat{\lambda}^h$

From (3), we note that each reconstructed pixel value is a linear combination of all the data. Thus, proving asymptotic multivariate normality of the scan distribution is equivalent to proving the asymptotic normality of a scaled sum of independent Poisson variates. This follows from

Theorem 2.1 *Let X_1, X_2, \dots, X_n be independent Poisson random variables with rate parameters $N\gamma_1, N\gamma_2, \dots, N\gamma_n$ respectively. Then, for any a_1, a_2, \dots, a_n , not all zero, as $N \rightarrow \infty$,*

$$\frac{\sum_{i=1}^n a_i X_i - \sum_{i=1}^n a_i N\gamma_i}{\sqrt{\sum_{i=1}^n a_i^2 N\gamma_i}} \xrightarrow{\mathcal{L}} N(0, 1) \quad (5)$$

Proof: From the Central Limit Theorem, we have

$$\frac{X_i - N\gamma_i}{\sqrt{N\gamma_i}} \xrightarrow{\mathcal{L}} N(0, 1); \quad i = 1, 2, \dots, n \quad (6)$$

as $N \rightarrow \infty$. The LHS of (5) reduces to,

$$\sum_{i=1}^n \sqrt{\frac{a_i^2 \gamma_i}{\sum_{i=1}^n a_i^2 \gamma_i}} \left(\frac{X_i - N\gamma_i}{\sqrt{N\gamma_i}} \right) \quad (7)$$

which is asymptotically standard normal, using (6) and Slutsky's Theorem.

Corollary 2.2 *As $N = \sum_j \mu_j \rightarrow \infty$, $\hat{\lambda}$ converges to a multivariate Gaussian distribution.*

Proof: Write $\mu_i = N\gamma_i$, $i = 1, 2, \dots, T$. Then any linear combination of $\hat{\lambda}^h$ is asymptotically Gaussian because it reduces to a linear combination of independent Poisson variates and the conditions of Theorem 2.1 apply. The result follows by Cramer-Wold Theorem.

The mean of $\hat{\lambda}^h$ is $S_h \lambda$. From (2), the dispersion matrix Σ of $\hat{\lambda}^h$ is given by,

$$\Sigma = S_h(K'K)^{-1}K'\text{Var}(y)K(K'K)^{-1}S_h \quad (8)$$

Reconstruction in PET is practical because Fast Fourier Transforms are used in the implementation.

This is not readily possible in the case of (8). So, we need approximation methods whereby reconstruction-type convolution procedures can be used in calculating dispersion.

2.1.3 Approximating Dispersion

Theoretically, using the Poisson nature of the observed counts, one can develop exact formulae for the variances of the reconstructed pixel values directly from (4) and obtain unbiased estimates by repeating the reconstruction procedure after replacing the kernel $e_h(\cdot)$ with its square $e_h^2(\cdot)$.

$$\hat{\sigma}_i^2 = \widehat{\text{Var}}(\hat{\lambda}_i^h) = \sum_{\theta, d} e_h^2(u_i \cos \theta + v_i \sin \theta - d) y_{d, \theta} \quad (9)$$

This was suggested by Alpert, *et. al.* [1]. In practice, (4) is implemented via discrete convolution through Fast Fourier Transforms. Interpolation steps are required during backprojection. Studies show that ignoring these over-approximates variances and can be corrected with negligible added computational effort ([9],[11]).

To approximate correlations, notice that if the variances of y are assumed uniform, (8) reduces to,

$$\text{Var}(\hat{\lambda}^h) \doteq \tilde{\Sigma} = \bar{\mu} S_h (K'K)^{-1} S_h, \quad (10)$$

where $\bar{\mu}$ is the assumed common variance of the observables. The approximately Toeplitz/Fourier form of $K'K$ (and hence, of $S_h (K'K)^{-1} S_h$) means that the correlation between the i 'th and j 'th reconstructed pixel values is,

$$\text{Corr}(\hat{\lambda}_i^h, \hat{\lambda}_j^h) = \frac{C_h(|i-j|)}{C_h(0)} \quad (11)$$

where $\Upsilon = \{C_h(0), C_h(1), \dots, C_h(I)\}$ is the first row of $S_h (K'K)^{-1} S_h$. Writing $\hat{\sigma} = \text{diag}(\hat{\sigma}_1, \hat{\sigma}_2, \dots, \hat{\sigma}_I)$, the estimated dispersion matrix is,

$$\hat{\Sigma} = \hat{\sigma} \frac{S_h (K'K)^{-1} S_h}{C_h(0)} \hat{\sigma} \quad (12)$$

Approximate variances of estimated mean activity over a region-of-interest (ROI) – estimated by a linear combination, $c' \hat{\lambda}$ – are estimated [11] by,

$$\begin{aligned} \widehat{\text{Var}}(c' \hat{\lambda}_h) &\cong (\hat{\sigma} c)' \frac{S_h (K'K)^{-1} S_h}{C_h(0)} (\hat{\sigma} c) \\ &= \sum_{\nu} |\check{\psi}_{\nu}|^2 \check{\Upsilon}_{\nu} \end{aligned} \quad (13)$$

In the above, $\check{\psi}$ is the Fourier Transform of $\psi = \hat{\sigma} c$, while $\check{\Upsilon}$ is the Fourier Transform of Υ .

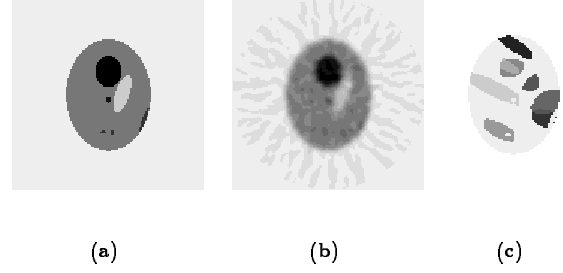


Figure 1: (a) The Vardi-Shepp phantom used in the simulations. (b) Sample reconstruction. (c) A few of the regions-of-interest used in the validations

2.2 Performance Evaluations

2.2.1 Simulation Experiments

The digitized Vardi-Shepp phantom (Figure 1a) was used in our experiment. This computer-generated artificial source distribution is made up of seven ellipses and is a simplified imitation of the brain's metabolic activity [18]. The imaging domain was subdivided into 128×128 pixels, while the observation domain had 128×320 distance-angle bins. Data were generated in the projection domain and reconstructions obtained using a filter with bandwidth set at 4 pixels. The filter resolution corresponds to moderate smoothing used in PET reconstruction. The expected number of total counts was set at $N = 3.16 \times 10^5$. 5000 reconstructions were obtained for use in our evaluations. A sample realization is shown in Figure 1b.

The performance of the dispersion formulae was evaluated in terms of the ability to approximate the standard deviations of reconstructed mean activities in elliptical regions (ROI) of uniform activity, of random orientation and size ranging from 6 to 787 pixels, drawn in the phantom. A few of these ROIs are shown in Figure 1c. The standard deviations of the estimated mean activities were estimated from the simulations and were used as the “ground truth”. Convolution formulae (13) were used in our approximations.

2.2.2 Results

The relative percent errors of the approximated standard deviations were calculated for purposes of our evaluation. These ranged from -10.7% to 25.1%, with mean -0.01%. Figure 2 is a plot of the percent errors in approximating ROI standard deviation. We notice that there is a slight under-approximation, consistent with the observation made in [3]. Further, while there is no identifiable pattern in the plot against the true (Figure 2a), the quality of the approximations deteriorates for regions farther away from the center of

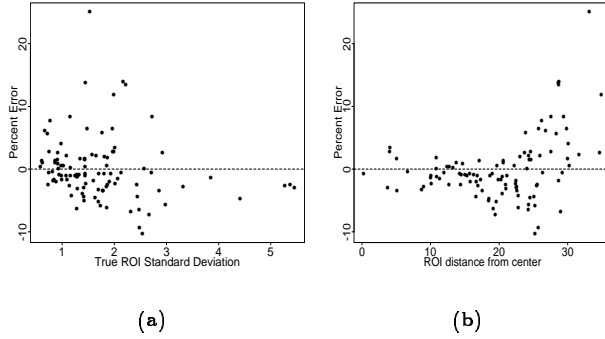


Figure 2: Percent relative errors in approximating ROI standard deviations against (a) true and (b) ROI distance from image center

the imaging region (Figure 2b). However, the computational appeal of using Fourier methods when simulating Gaussian random fields leads us to adopt this correlation structure in this application.

In addition, the approximate multi-Gaussian distributional assumption of reconstructed PET scans was tested and found reasonable for a range of realistic total expected counts [10].

3 Functional Image Variances

Local tissue metabolism has usually been assessed from dynamic PET scans by modeling locally averaged time-course measurements [15]. Functional imaging techniques, like mixture analysis [12], generate more comprehensive pixel-wise representations.

3.1 Mixture Models

Let $\lambda_i(t)$ represent the true source distribution in the t 'th time-bin at the i 'th pixel in the PET imaging domain. The vector $\lambda_i(\cdot) = \{\lambda_i(t); t = 1, 2, \dots, T\}$ is called the true *time-activity curve* (TAC) at the i 'th pixel. A K -component mixture model represents the i 'th pixel TAC as a weighted average of K underlying curves (sub-TACs), $\xi_k, k = 1, 2, \dots, K$.

$$\lambda_i(t) = \sum_{k=1}^K \pi_{ik} \xi_k(t) \quad (14)$$

where the mixing proportions $\{\pi_{ik}; k = 1, 2, \dots, K\}$ lie in the K -dimensional simplex. The physical basis for such a representation is that the sub-TACs (ξ 's) correspond to the different tissue types represented in the image and the underlying π_i 's indicate the anatomic tissue composition of the underlying pixel.

Functional imaging maps a metabolic parameter of interest, ϑ , at each pixel in the image. The mixture

analysis approach fits the metabolic parameter $\vartheta^{(k)}$ to each tissue sub-TAC $\xi_k(\cdot)$ and following (14) regards each pixel biologic parameter as a composition of the component tissue parameters,

$$\vartheta_i = \sum_{k=1}^K \pi_{ik} \vartheta^{(k)} \quad (15)$$

3.1.1 Estimation Algorithms

For functional imaging, the data are a time-course sequence of reconstructed PET scans $\hat{\lambda}^h = \{\hat{\lambda}^h(t); t = 1, 2, \dots, T\}$. The number of tissue types, K , the sub-TACs $\xi_k(\cdot)$, and the mixing proportions π_{ik} 's have to be determined. K is obtained from anatomic considerations or through clustering or other sophisticated algorithms ([12],[14]). Estimation of ξ 's and π 's are usually done alternately to fit the model,

$$\hat{\lambda}_i^h(t) \sim \sum_{k=1}^K \pi_{ik} \xi_k(t); \quad t = 1, 2, \dots, T. \quad (16)$$

The problem of estimating ξ 's, given the π 's, is a low-dimensional problem and usually robust to the choice of the estimation method. On the other hand, the dimensionality of the π_{ik} 's is high and so the estimation problem is delicate. Many methods have been proposed: among them is a quadratic (weighted) least-squares algorithm which constrains π_{ik} 's to belong to the K -dimensional simplex.

The tissue metabolic parameters $\vartheta^{(k)}$'s are estimated from the $\xi_k(\cdot)$'s and the pixel metabolic parameters are estimated following (15),

$$\hat{\vartheta}_i = \sum_{k=1}^K \hat{\pi}_{ik} \hat{\vartheta}^{(k)} \quad (17)$$

3.1.2 Assessing Variability

Analytic expressions for $\text{Var}(\hat{\vartheta})$ are intractable because of the nonlinear methods used in the extraction. The prohibitive cost of generating time-course sequences from realizations in the observation domain makes the usual resampling approach impractical. A modified simulation approach may be employed by using the results of Section 2 and the independence of PET scans over time-points. Time-course sequences are then practical to simulate in the imaging domain from this approximate multi-Gaussian model. These are used to generate bootstrap samples for the ϑ 's from where variability can be assessed.

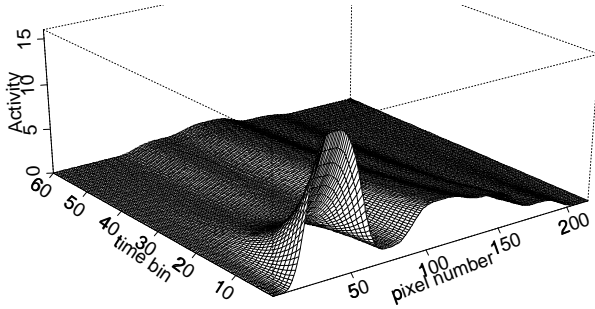


Figure 3: Perspective plot of the source distribution $\lambda(\cdot)$ used in the experiments.

3.2 Performance Evaluations

3.2.1 One-dimensional Experiments

Experiments were conducted to assess the performance of the suggested approach in estimating the pixel-wise variances of the ϑ 's. Since it is not possible to estimate the true variances in a two-dimensional PET setup, evaluations were done in a simplified one-dimensional deconvolution setting [13] with characteristics matching PET reconstruction. A 6-component mixture model was specified. In this set-up, ξ 's (and hence $\vartheta^{(k)}$'s) were assumed known. The source distribution $\lambda(\cdot)$ (Figure 3) was specified using (14) with mixing proportions (π_{ik} 's) that are blurred step functions [4].

Time activity curves over 60 time-points were reconstructed at 216 bins (pixels) from realizations of a inhomogeneous Poisson process in the observation domain [4]. The reconstructions were smoothed by a Gaussian kernel with bandwidth preset to correspond to smoothing parameters that are reasonable for the given total expected number of emissions. The π_{ik} 's were estimated from $\hat{\lambda}^h(\cdot)$ and used to obtain $\hat{\vartheta}$'s.

1000 simulated reconstructions of the TAC were obtained by simulating the observed process and $\hat{\vartheta}$'s were extracted from each $\hat{\lambda}^h(\cdot)$. Sample pixel-wise standard deviations of these $\hat{\vartheta}_i$'s are assumed to be the truth in our performance evaluations.

Realizations were simulated from the approximate multi-Gaussian model for the estimated TACs $\hat{\lambda}^h(\cdot)$. Bootstrap samples of $\hat{\vartheta}$'s were obtained as outlined in Section 3.1.2 and standard deviations calculated. The experiment was done with bootstrap sample sizes $m=10, 30$ and replicated 500 times in order to study the distributional properties of these bootstrapped standard deviations.

The above experiments were performed for low (1.02×10^5), medium (2.05×10^5) and high (4.1×10^5) expected total counts, $\sum_{i,t} \lambda_i(t)$. Corresponding bandwidths for the smoothing kernel were set at 9.7, 8.4

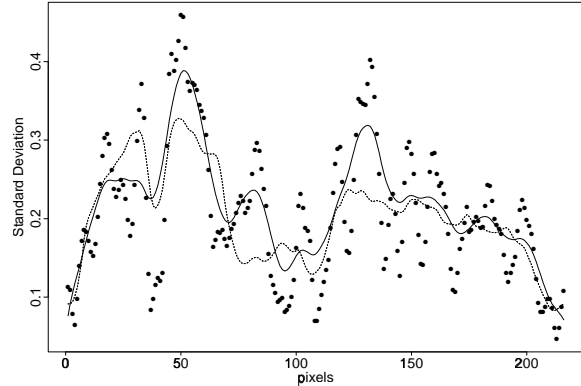


Figure 4: True standard deviation (broken line) and its unsmoothed (points), and smoothed (bold line) bootstrap estimates (10 bootstrap replications).

Counts ($\times 10^5$)	Bias		Variability	
	10 rep	30 rep	10 rep	30 rep
1.02	4.6 (5.6)	4.8 (3.7)	17.3 (27.7)	14.0 (21.6)
2.05	5.1 (3.8)	5.1 (5.4)	16.1 (27.6)	12.9 (21.3)
4.10	5.1 (5.3)	4.9 (3.7)	15.5 (27.3)	12.3 (21.0)

Table 1: Bias and variability measures for smoothed bootstrap standard deviation estimates over different total expected counts and bootstrap sample sizes. The bias measure is the percent relative bias averaged over pixels and the variability measure is the mean relative percent absolute error in estimating standard deviations averaged over pixels. Corresponding measures for unsmoothed estimates are in parenthesis.

and 7.8 pixels. (Different expected total counts can be interpreted as different dosage levels of the radio-tracer.)

3.2.2 Results

The percent relative absolute bias, averaged over pixels was about 4-5% for all count rates and bootstrap sample sizes. Figure 4 shows a set of pixel-wise bootstrapped standard deviation estimates (points). Here $m=10$. Naive smoothing of the estimates was done using the variable-span smoother of Friedman [6] which uses a local cross-validation scheme to obtain the smoothing bandwidth. The smoothed estimate (Figure 4, bold line) is shown to give a better fit. Variability of the estimates was measured by the average, over pixels, of the mean percent absolute error in estimating standard deviation. Table 1 summarizes the bias and the variability measures of the estimated bootstrap standard deviations. The percent relative absolute biases are not altered appreciably as a result of the smoothing; however, the variability measures are considerably improved. It is observed that the bias

and error rates do not differ appreciably for different total expected counts. However, as expected, the error rates decrease with increasing bootstrap sample size.

4 Discussion

The main contributions of this paper can be broadly categorized into two parts. The first (Section 2) specifies that the distribution of a reconstructed PET scan is approximately multivariate normal. This section also suggests practical algorithms for computing accurate variability approximations, using convolution-type algorithms. While there is some room for improvement here, this in itself is a major contribution to the field. The second contribution (Section 3) is a practical approach towards variability assessment in functional images. This section builds on the theoretical framework of Section 2 to make a simulation approach through a modified bootstrap possible. Preliminary results reported here are very encouraging. We have addressed the problem of estimating pixel-wise variances of functional images; the technique can be easily extended to assess other variability measures like correlations. Also, the method can be applied to functional imaging techniques other than mixture analysis.

A number of issues remain to be addressed. In smoothing bootstrap standard deviation estimates, the variable-span fitting algorithm of Friedman [6] has been used. Obtaining the smoothing bandwidth by local cross-validation may under-smooth in the presence of positively correlated variates. Hence, the obtained error rates may potentially be decreased by a more sophisticated choice of smoothing parameter. Another question of interest is determining the number of bootstrap samples. Hence, while this seems a promising new technique towards variability estimation in functional images, a number of issues remain to be investigated.

References

- [1] Alpert, N. M., Chesler, D. A., Correia, J. A., Ackerman, R. H., Chang, J. H., Finklestein, S., Davis, S. M., Brownell, G. L., and Taveras, J. M., "Estimation of the local statistical noise in emission computed tomography", *IEEE Trans. Med. Imag.*, MI-1:142-146, 1982.
- [2] Blomqvist, G., Eriksson L., Rosenqvist G., "The effect of spatial correlation on the quantification in Positron Emission Tomography" *Neuroimage*, 2:2, 1995.
- [3] Carson, R. E., Yan, Y., Daube-Witherspoon, M. E., Freedman, N., Bacharach, S. L. and Herscovitch, P., "An Approximation Formula for the Variance of PET Region-of-Interest Values", *IEEE Trans. Med. Imag.*, 12:240-50, 1993.
- [4] Choudhury, K. R. and O'Sullivan, F., "A Statistical Examination of FBP and ML for Estimating Mixture Models from Dynamic PET Data", *1995 IEEE Nucl. Sci. Symp. and Med. Imag. Conf. Record*, 3:1237-41, 1995.
- [5] Efron, B., "The Jackknife, the Bootstrap and Other Resampling Plans", SIAM, 1982.
- [6] Friedman, J. H., "A variable span smoother", *Tech. Rep. No. 5, Lab. for Comp. Stat., Dept. of Stat., Stanford Univ., Stanford, CA*, 1984.
- [7] Haynor, D. R. and Woods, S. D., "Resampling Estimates of Precision in Emission Tomography", *IEEE Trans. Med. Imag.*, 8:337-43, 1989.
- [8] Huesman, R. H., "A new fast algorithm for the evaluation of regions of interest and statistical uncertainty in computed tomography", *Phys. Med. Biol.*, 29:543-52, 1984.
- [9] Maitra, R. and O'Sullivan, F., "Estimating the Variability of Reconstructed PET Data : A Technique Based on Approximating the Reconstruction Filter by a sum of Gaussian kernels", *1995 IEEE Nucl. Sci. Symp. and Med. Imag. Conf. Record*, 3:1411-14, 1995.
- [10] Maitra, R., Variability Estimation in Linear Inverse Problems. *Ph. D. dissertation*, Department of Statistics, University of Washington, 1996.
- [11] Maitra, R. and O'Sullivan, F., "Variability Estimation in Inverse Problems", in prep.
- [12] O'Sullivan, F., "Imaging radiotracer model parameters in PET : A mixture analysis approach", *IEEE Trans. Med. Imag.*, 12:399-412, 1993.
- [13] O'Sullivan, F., Pawitan, Y. and Haynor, D., "Reducing Negativity Artifacts in Emission Tomography: Post-Processing Filtered Backprojection Solutions", *IEEE Trans. Med. Imag.*, 12:653-663, 1993.
- [14] O'Sullivan, F., "Metabolic images from dynamic Positron Emission Tomography studies", *Stat. Meth. in Med. Res.*, 3:87-101, 1994.
- [15] Phelps, M. E., Huang, S. C., Hoffman, E. J., Selin, C., Sokoloff, L., and Kuhl, D. E., "Tomographic measurement of local cerebral glucose metabolic rate in humans with [F-18]2-Fluoro-2-deoxy-D-glucose: validation of method", *Ann. Neurol.* 6:371-388, 1979.
- [16] Snyder, D. L., Thomas, L. J., and Ter-Porgossian, M. M., "A mathematical model for positron emission tomography system having time of flight measurement", *IEEE Trans. Nucl. Sci.*, 28:3575-81, 1981.
- [17] Ter-Porgossian, M. M., Raichle, M. E. and Sobel, B. E., "Positron Emission Tomography", *Scientific American*, 243(4):170-181, 1980.
- [18] Vardi, Y., Shepp, L. A. and Kaufman, L. A., "Statistical model for positron emission tomography", *J. Amer. Statist. Assoc.*, 80:8-37, 1985.